Real-Time experimental demonstration of DSP-enabled soft-ROADMs with multi-level flexible add/drop functions for cloud access networks

Al-Rawachy, Ehab; Giddings, Roger; Tang, Jianming

Optics Express

DOI:
10.1364/OE.27.000016

Published: 07/01/2019

Peer reviewed version

Real-Time experimental demonstration of DSP-enabled soft-ROADMs with multi-level flexible add/drop functions for cloud access networks

E. AL-RAWACHY,[1,2] R. P. GIDDINGS,[1,*] AND J. M. TANG[1]

1. School of Electronic Engineering, Bangor University, Dean Street, Bangor, LL57 1UT, UK
2. College of Electronics Engineering, Electronics department, Ninevah University, Mosul, Iraq
[*] r.p.giddings@bangor.ac.uk

Abstract: Making use of digital filtering, drop RF signal-driven intensity modulation and passive optical coupling, DSP-enabled flexible ROADMs, termed soft-ROADMs, are experimentally demonstrated in real-time, which are free from both optical filters and O-E-O conversions and are inherently transparent to major network design characteristics. In a 4-channel IMDD optical network node incorporating FPGA-based orthogonal digital filter multiplexing, fully real-time soft-ROADM dynamic add and drop operations at both sub-wavelength and spectrally overlapped orthogonal sub-band levels are extensively, experimentally explored, along with their performance robustness against condition variations of practical networks associated with low-cost optical/electrical components. It is shown that the soft-ROADMs introduce optical power penalties as low as 1.4dB for add operation and 2dB for drop operation. For received optical powers fixed at -10dBm, the add operation can tolerate a differential optical input dynamic range of 6.5dB (1.5dB) for sub-wavelength (sub-band) add operation. On the other hand, robust drop operation performances are obtainable over a ~5dB (16°) drop RF signal amplitude (phase) variation range. This work is a significant milestone in demonstrating the technical feasibility of utilising soft-ROADMs to create a programmable networking environment capable of addressing elastic 5G slicing and the SDN paradigm.

OCIS codes: (060.2330) Fiber optics communications; (060.2360) Fiber optics links and subsystems; (060.4230) Multiplexing.

References and links

[1] J.M. Senior, P.Kourtessis, M. Milosavljevic, andW. Lim, "OFDMA-PON for future generation metro-access networks," in Proc. Photon. Global Conf., Dec. 2012, pp. 1–5.
[2] M.Xia,Y.Owada, M. Inoue, and H. Harai, "Multiple-gateway deployment for wired/wireless converged access networks," in Proc. IEEE 4th Int. Symp. Adv. Netw. Telecommun. Syst., Dec. 2010, pp. 79–81.
[3] J. I. Kani, S. Kuwano, and J. Terada, "Options for future mobile backhaul and fronthaul," Opt. Fiber Technol. **26**, 42–49 (2015).
[4] T. Watanabe, K. Suzuki, T. Goh, K. Hattori, A. Mori, T. Takahashi, T. Sakamoto, K. Morita, S. Sohma, and S. Kamei, "Compact PLCbased transponder aggregator for colorless and directionless ROADM," presented at the Optical Fiber Communication Conf. Expo., Nat. Fiber Optic Engineers Conf., Los Angeles, CA, USA, Mar. 2011, Paper OTuD3.
[5] W. I.Way, "Optimum architecture for M×N multicast switch-based colorless directionless, contentionless, and flexible-grid ROADM," presented at theOptical Fiber Communication Conf. Expo.,Nat. FiberOptic Engineers Conf., Los Angeles, CA, USA, Mar. 2012, Paper NW3F.5.
[6] R. A. Jensen, "Optical switch architectures for emerging colorless/directionless/contentionless ROADM Networks," presented at the Optical Fiber Communication Conf. Expo., Nat. Fiber Optic Engineers Conf., Los Angeles, CA, USA, Mar. 2011, Paper OThR3
[7] W. I.Way, "Next generation ROADMarchitectures," presented at the Asia Communications Photonics Conf., Guangzhou, China, Nov. 2012, Paper AS1G.3.
[8] M. D. Feuer, S. L. Woodward, P. Palacharla, X. Wang, I. Kim, and D. Bihon, "Intra-node contention in

dynamic photonic networks," J. Lightw. Technol., **29**(4), 529–535 (2011).
[9] W. I. Way, P. N. Ji, and A. N. Patel, "Wavelength contention-free via optical bypass within a colorless and directionless ROADM [Invited]," J. Opt. Commun. Netw., **5**(10), A220–A229 (2013).
[10] Z. Shen, H. Hasegawa, K. Sato, T. Tanaka, and A. Hirano, "A novel semi-flexible grid optical path network that utilizes aligned frequency slot arrangement," presented at the 39th European Conf. Optical Communication, London, U.K., Sep. 2013, Paper We.2.E.2.
[11] S. L.Woodward and M. D. Feuer, "Benefits and requirements of flexiblegrid ROADMs and networks [Invited]," J. Opt. Commun. Netw., **5**(10), A19–A27 (2013).
[12] W. Jin, X. Duan, M. Bolea, R. Giddings, N. Jiang, C. Zhang, K. Qiu, and J. Tang, "New ROADMs with DSP-Enabled Dynamic and Flexible Operations for Elastic Optical Networks," OFC 2015, paper. Th2A.50.
[13] W. Jin, X. Duan, Y. Dong, B. Cao, R. P. Giddings, C. Zhang, K. Qiu, and J. M. Tang, "DSP-Enabled Flexible ROADMs Without Optical Filters and O-E-O Conversions," J. Light. Technol. **33**(19), 4124–4131 (2015).
[14] W. Jin, C. Zhang, X. Duan, M. R. Kadhum, Y. X. Dong, R. P. Giddings, N. Jiang, K. Qiu, and J. M. Tang, "Improved Performance Robustness of DSP-Enabled Flexible ROADMs Free from Optical Filters and O-E-O Conversions," IEEE/OSA J. Opt. Commun. Netw. **8(8)**, 521-529 (2016).
[15] X. Duan, M. L. Deng, W. Jin, R. P. Giddings, S. Mansoor, and J. M. Tang, "Experimental Demonstration of DSP-enabled Drop Operations of Flexible ROADMs Excluding Optical Filters and O-E-O Conversions," OFC 2016, paper M3E.4.
[16] E. Al-Rawachy, R. P. Giddings, and J. M. Tang, "Experimental Demonstration of Real-Time Add/Drop Operations in DSP-enabled Flexible ROADMs for Converging Fixed and Mobile Networks," OFC 2018, paper W2A.33.
[17] M. Bolea, R. P. Giddings, and J. M. Tang, "Digital orthogonal filter-enabled optical OFDM channel multiplexing for software-reconfigurable elastic PONs," J. Light. Technol. **32**(6), 1200–1206 (2014).
[18] M. Bolea, R. P. Giddings, M. Bouich, C. Aupetit-Berthelemot, and J. M. Tang, "Digital Filter Multiple Access PONs With DSP-Enabled Software Reconfigurability," J. Opt. Commun. Netw. **7**(4), 215-222 (2015).
[19] Y. Li, et.al., "tSDX: enabling impairment-aware all-optical inter-domain exchange", J. Light. Technol. **36**(1), 142-154 (2017).
[20] Y. Li, et.al., "Transparent software-defined exchange (tSDX) with real-time OSNR-based impairment-aware wavelength path provisioning across multi-domain optical networks", OFC 2017 , Paper Th5A.2.
[21] R. M. Dorward, M.J. Anderson, R. P. Giddings, "Technical and market feasibility of high-speed software-reconfigurable OOFDM/DFMA-based Optical transceivers for Next Generation Access Network PONs," ICTON 2016; Paper Th.B1.4.
[22] X. Duan, R.P. Giddings, M. Bolea, Y. Ling, B. Cao, S. Mansoor, and J.M. Tang, "Real-time experimental demonstrations of software reconfigurable optical OFDM transceivers utilizing DSP-based digital orthogonal filters for SDN PONs," Opt. Express **22**(16), 19674-19685 (2014).
[23] X. Q. Jin and J. M. Tang, "Experimental Investigations of Wavelength Spacing and Colorlessness of RSOA-Based ONUs in Real-Time Optical OFDMA PONs," J. Light. Technol. **30**(16), 2603–2609 (2012).
[24] X. Duan, R. P. Giddings, S. Mansoor, and J. M. Tang, "Performance Tolerance of IMDD DFMA PONs to Channel Frequency Response Roll-Off," IEEE Photonics Technol. Lett. **29**(19), 1655–1658 (2017).
[25] E. Al-Rawachy, R. P. Giddings, and J. M. Tang, "Experimental demonstration of a DSP-based cross-channel interference cancellation technique for application in digital filter multiple access PONs," Opt. Express **25**(4), 3850–3862 (2017).
[26] A. J. Lowery, "Improving Sensitivity and Spectral Efficiency in Direct-Detection Optical OFDM Systems," in OFC/NFOEC 2008, paper OMM4.

1. Introduction

Cloud access networks (CANs) have been proposed [1-2] as a cost-effective "future-proof" network solution to not only meet the ever-increasing growth in data traffic capacity, but also to effectively support an increasing range of dynamic traffic types with widely varying characteristics. To significantly reduce the total cost of network ownership, CANs also target the seamless integration of traditional optical access networks, metropolitan area optical networks and 4G/5G mobile front-haul (MFH)/back-haul (MBH) networks [3]. In addition, to achieve sustainable business models for network operators, offering advanced services such as the rapid provision of on-demand, client-specific network interconnectivities is desirable, which requires that CANs have to be highly adaptive, resource-efficient and dynamically reconfigurable. To meet these requirements, CANs must be equipped with a vital networking function namely software-defined networking (SDN)-based, dynamic on-line network reconfigurability and bandwidth provisioning with fine granularity, which has to be performed at wavelength, sub-wavelength and/or sub-band levels. Furthermore, to achieve ultra-high flexibility and elasticity in network provisioning, CANs are also envisaged to transparently

accommodate a diverse range of important network design features such as signal modulation formats, signal detection schemes, flexible WDM grids, diversified network topologies and multiple access techniques.

Reconfigurable optical add/drop multiplexers (ROADMs) are one of the most important networking elements that will play a vital role in the practical realisation of highly versatile CANs delivering the aforementioned networking features. For cost-sensitive CAN applications, ROADMs must be highly cost effective in terms of both capital equipment/installation costs and operational costs. There has been many recent developments in ROADM technologies, which provide advanced features over conventional technologies, these include i) colourless operation achieved using optical components such as tuneable optical filters [4] and tuneable coherent transponders [5], ii) directionless operation by the use of broadcast and select architectures [5]–[7], iii) contentionless operation by the use of optical transponders cascaded with optical switches [8] or extra contention-resolution banks [9] and iv) flexible-grid ROADMs enabled by filterless coherent transponders [5], tuneable optical filters [10] and flexible-grid wavelength-selective switches [11]. However, existing ROADMs and the emerging advances in technology mainly target long haul optical backbone networks and only provide advanced wavelength level switching functionalities in term of the aforementioned colorlessness, directionlessness, contentionlessness and WDM gridlessness [4-11]. As a direct result of such course wavelength-level switching functions and their associated high equipment costs, those ROADMs are therefore incompatible with cost-sensitive CANs of interest in the present paper. As such, cost-effective ROADMs that can provide flexible channel switching at all of the aforementioned three levels and that are fully compatible with SDN-based network control are an essential required for implementing highly reconfigurable, elastic and transparent CANs.

To address such an unprecedented technical challenge, we have recently proposed low-cost digital signal processing (DSP)-enabled optical-domain ROADMs, termed here soft-ROADMs [12-14]. The proposed soft-ROADM operations are independent of the underlying signal and channel characteristics, so the soft-ROADMs are highly versatile in their applications in CANs. The soft-ROADMs have very simple architectures comprising of passive optical coupler-based add elements and intensity modulation (IM)-based drop elements without incorporating either costly narrowband optical tunable band pass-filters (OTBPFs) or optical-electrical-optical (O-E-O) signal conversions [12-14]. Enabled by DSP, the soft-ROADM provides SDN-controllable, dynamic and flexible optical switching at wavelength, sub-wavelength and spectrally-overlapped orthogonal sub-band levels, in intensity modulation and direct detection (IMDD)-based networks incorporating embedded Hilbert-pair-based digital orthogonal filters in terminal equipment transceivers (TETs), whilst still maintaining excellent transparency to various network features. The performance of the soft-ROADM has been comprehensively investigated using numerical simulations [12-14] and its drop operation has also been experimentally demonstrated using an off-line DSP receiver [15]. More recently the basic technical feasibility of both the add and drop functions at sub-band level have been demonstrated in an experimental system employing a real-time soft-ROADM [16].

As a significant extension to the real-time experimental demonstration in [16], the work presented in this paper further validates the technical feasibility of the proposed soft-ROADM in a fully real-time system consisting of four independent and guard-band free, digital orthogonal filtering multiplexed channels in terms of dynamically switching signals in real-time at sub-wavelength and spectrally-overlapped orthogonal sub-band levels. In addition, compared to [16] this paper also rigorously evaluates the soft-ROADM's physical-layer dynamic performance and its robustness in terms of: i) add operation tolerance to differential optical power for various add operation combinations, and ii) drop operation tolerance to variations in the characteristics of the drop RF signal (used to select the drop channel). As such, this paper provides some further deeper insights into the technical aspects associated with the application of the soft-ROADMs in CAN scenarios. For an adopted forward error correction

(FEC) limit of 1.0×10^{-3}, it is shown that the soft-ROADM induces maximum power penalties of just 1.4dB and 2dB for the add and drop operations, respectively. Furthermore, to maintain all channel bit error rates (BERs) below the adopted FEC limit, the add operation can tolerate a maximum differential optical power dynamic range of 6.5dB (1.5dB) for sub-wavelength (sub-band) add operation, and the drop operation can tolerate variations in the drop RF signal's amplitude of 5dB and its phase of 16°. The results indicate that the proposed soft-ROADM exhibits good tolerance to variations in practical network operating conditions.

2. Soft-ROADM architecture and operating principle

2.1 Generation of wavelength, sub-wavelength and sub-band channels

The CAN optical layer consists of three distinct channel levels. The top level is the wavelength level as in a typical WDM-based optical network, with each wavelength consisting of two different sub-levels of sub-channels [17,18]: the upper sub-level consists of multiple sub-wavelength (Sub-λ) bands located at different RF center frequencies (CFs), and the lower sub-level is formed by each Sub-λ band consisting of two spectrally overlapped orthogonal sub-bands (Sub-B) with their associated RF carriers located at the same CF but with a relative phase difference of 90°, these sub-bands are therefore orthogonal and are denoted as I and Q (In/Quadrature-phase). A full explanation of the generation of the digital orthogonal filtering-multiplexed Sub-λ and Sub-B channels is presented in [18].

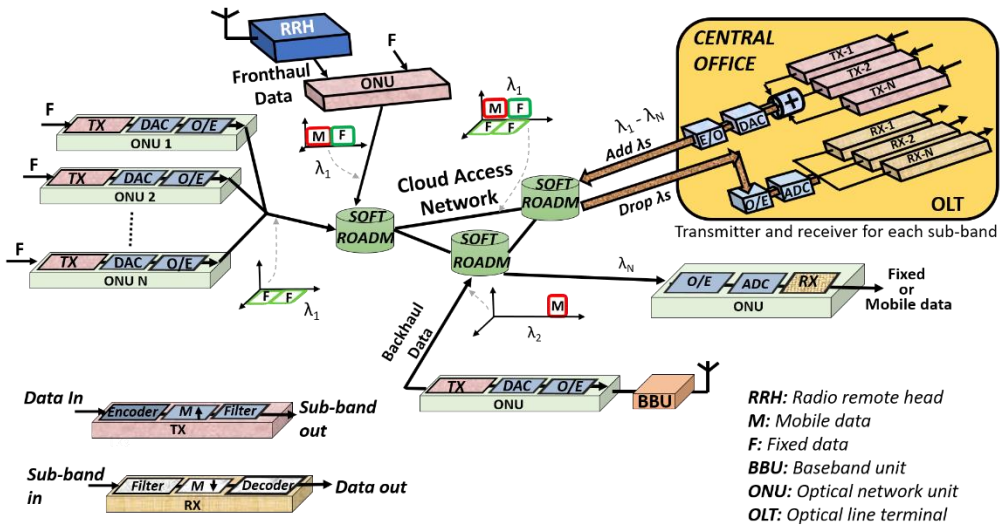

Fig. 1. DSP enabled soft-ROADMs in a cloud access network.

Figure 1 illustrates an example of a CAN employing soft-ROADM-based channel switching at all of the aforementioned three channel levels. The soft-ROADM providing on-line reconfigurable connectivity between an optical line terminal (OLT) in the central office and various optical network units (ONUs) to transparently support both fixed and/or mobile traffic. The CAN is also able to dynamically provision fronthaul links between BBUs and RRHs physically located at different sites in the CAN. Although 5G is just one of many network scenarios supported by the CAN, it is important to highlight some key features of the digital orthogonal filter-based channel multiplexing technique and the soft-ROADM-enabled channel switching technique to illustrate the potential performance characteristics of a CAN and thus the alignment with the targeted requirements of 5G mobile networks:

- **Higher system capacity:** The technique can support a large number of aggregated elastic channels, which is highly scalable. The soft-ROADM can also transparently accommodate different channel bandwidths achieved using various signal modulation formats including advanced modulation formats with high spectral efficiency. The wide channel bandwidth dynamic range with fine granularity allows more efficient use of the available network resources as statistical multiplexing can be fully exploited. The bandwidth of available ADC/DACs is perhaps the key bottleneck in terms of maximum per wavelength capacity, however the latest generation of converter technologies offers sampling rates in excess of 100GS/s.
- **Massive device connectivity:** The highly elastic channels with fine granularity, combined with inherent transparency to multiple access techniques and modulation formats, allows for a high count of low bandwidth connections.
- **Reduced latency:** As the soft-ROADM operates purely in the optical domain, the soft-ROADM operation-induced latency can be considered as negligible.
- **Low-cost:** The soft-ROADMs completely avoid expensive and bulky optical filters and O-E-O conversions, which significantly reduces overall cost
- **Energy saving:** The data carrying signals do not require conversion and processing in the electrical domain in order to add and drop sub-wavelength/sub-band channels, consequently this results in a huge saving in power consumption, as high speed electronic switching circuits are completely eliminated.

It is also interesting to highlight the backwards compatibility of the soft-ROADM with existing ITU-T and IEEE standards-based networks and transmission technologies, which permits a gradual migration to a CAN from the existing networks. There are three key aspects of backwards compatibility to highlight, i) full compliance with the ITU-T WDM grid which allows interoperability with conventional fixed-grid ROADMs, ii) whole wavelengths can be added and dropped allowing wavelengths carrying conventional optical signals to be switched by the soft-ROADM, and iii) the channels are transparent to modulation format so signals adopting standardized modulation formats can be transported. More specifically, the soft-ROADM in combination with a CDC architecture is also expected to be compliant to the ITU-T G.672 multi-degree ROADM characteristics at wavelength level.

2.2 Soft-ROADM architecture

As full details of the soft-ROADM architecture are given in [13], only its basic architecture is therefore outlined here. In the soft-ROADM, as illustrated in Fig. 2, the incoming WDM optical signal at the aggregated input port is first demultiplexed into separate wavelengths via an arrayed waveguide grating (AWG). Each wavelength is split into two parts via an optical splitter, the first part of each wavelength then passes through a drop element, where a targeted Sub-B (TSB) channel can be dropped to a drop port. Multiple drop elements are thus required for each wavelength, however the drop elements are colourless so all drop elements are identical. The second part of the wavelength then passes through an add element, where one or more channels, fed into an add port, can be added to the pass-through channels, before multiplexing the wavelength into the WDM output signal via an AWG. Similar to conventional ROADMs, additional WDM demultiplexing/multiplexing can also be implemented at the add/drop ports. The architecture in Fig. 2 depicts the West-East traffic direction, however the East-West direction would be implemented in a similar manner forming a 2-degree ROADM. As the soft-ROADMs would typically be configured in a ring architecture, as shown in Fig. 1, 2-degrees of switching is sufficient to allow low cost, flexible and dynamic allocation of the aggregated ring capacity throughout the CAN. It is perfectly feasible, however, to construct multi-degree soft-ROADMs by employing a broadcast and select architecture [5] in the express paths based on 1xN (N=degree) power splitters (PS) and wavelength selective switches (WSSs).

Furthermore, the broadcast and select architecture inherently supports directionless operation. Generally speaking, the soft-ROADMs in combination with the CDC architecture can support similar wavelength-level network performances as conventional ROADMs. However, it should be emphasised that soft-ROADMs are designed to provide optical add/drop operations at sub-wavelength and/or sub-band levels, which provide fine granularity, elastic sub-channels below the wavelength level, essential for the targeted CAN applications.

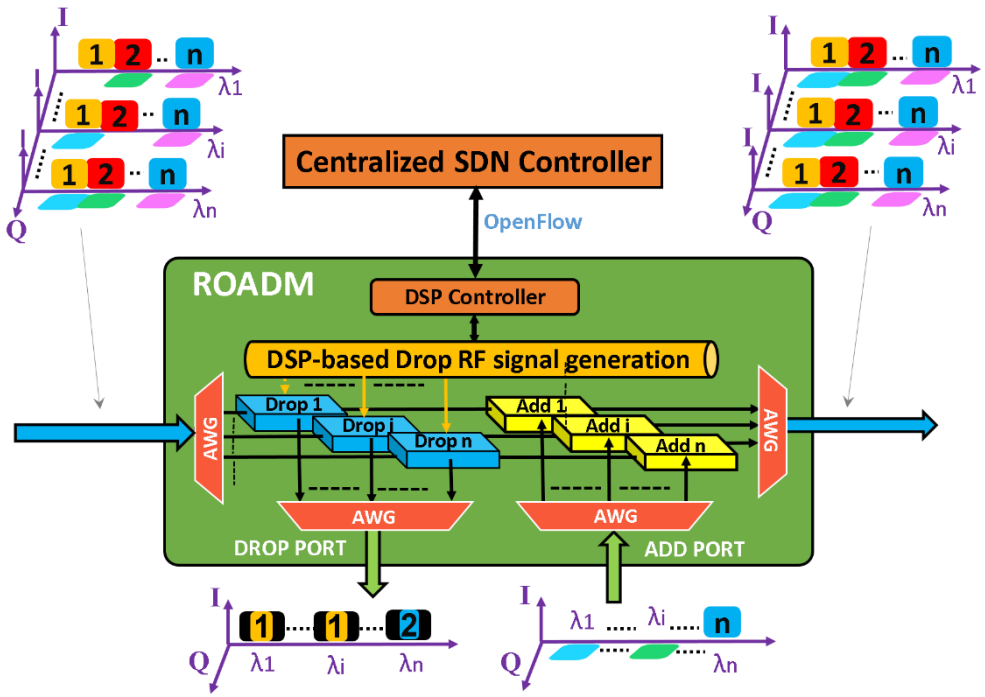

Fig. 2. Block diagram of basic soft-ROADM architecture.

The use of AWGs, as shown in Fig. 2, makes the soft-ROADM colorless at sub-wavelength levels only, however, utilizing WSSs would achieve colorlessness at the wavelength level also. Furthermore, as the contentionless feature is controlled by the SDN control plane, it is thus feasible to implement soft-ROADMs with colorless, directionless and contentionless (CDC) functionality. To dynamically configure the required network interconnectivity, a centralized SDN controller communicates, via a protocol such as extended OpenFlow, with embedded DSP controllers in the soft-ROADMs and the TETs using an approach presented in [13-14]. The required signaling channel could be implemented as an optical supervisory channel (OSC) carried by a dedicated wavelength outside the WDM wavelength band, as is the case in conventional ROADM technologies. Alternatively, a low bandwidth sub-band channel embedded in a multi-channel wavelength could potentially be employed as the signaling channel.

Network latency is a critical factor in CANs supporting 5G traffic. Minimisation of network latency can be achieved by employing soft-ROADMs with a CDC architecture in combination with a low latency enabled control plane such as a hierarchical SDN control architecture [19,20]. For cases where the order and sequencing of the dropped channels may be necessary, the adoption of the strategies reported in [19,20] can further reduce the network latency.

It is also important to highlight the fact that the drop and add elements each impose a 3dB loss in optical power on the pass-through wavelengths, the combined 6dB loss is comparable

to a conventional ROADM. This implies that the scalability of the soft-ROADM is similar to the conventional ROADM. However, the performance of concatenated soft-ROADMs is still an important area to be studied to assess for example i) the tradeoff between the number of soft-ROADMs and the overall CAN performance, and ii) the need and application of optical amplifiers in various CAN scenarios.

Other practical factors influencing the scalability of the soft-ROADM architecture are also important to consider. For a specific application scenario, the maximum wavelength-count is only restricted by the employed AWG or WSS devices. The aggregated signal bandwidth is ultimately limited by the bandwidth of the DAC/ADCs embedded in the TETs, as discussed in Section 2.1. Maximum Sub-λ channel count on a single wavelength is limited by DSP implementation complexity in the TETs, however, the DSP complexity due to the channel filtering does not scale linearly with channel count [21], in fact DSP complexity can reduce with channel count [21] as each transceiver processes a narrower bandwidth channel. For the case of a soft-ROADM dropping multiple channels to a PON with multiple ONUs, the ONU-count dependent performance of the PON has been investigated in [18] which showed that aggregated PON capacity is virtually independent of ONU-count and minimum received optical power increases by 1.7 dB when the number of ONUs is doubled, which is very similar to that observed in orthogonal frequency-division multiple access (OFDMA) PONs.

2.3 Soft-ROADM add operation

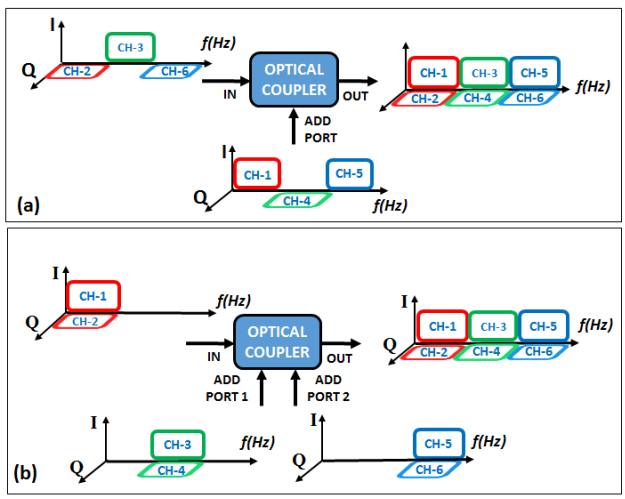

Fig. 3. Add operations with example signal spectra. (a) Sub-B add operation with single add port, (b) Sub-λ add operation with multiple add ports.

A simple passive optical coupler (OC) performs the add operation by simply adding the involved channels passively in the optical domain. Fig. 3 illustrates two representative examples of different add operation cases. An SDN controller configures the associated TETs' DSP to locate their channel(s) at a free location(s) in a specific wavelength's digital filtering space to avoid possible channel contention in the add element. A two-port optical coupler would be utilized to add the soft-ROADM's pass-through optical signal to a single tributary input signal as shown in Fig. 3(a). It is also feasible to use a multi-port coupler to add multiple signals simultaneously to the pass-through signal, thus providing a soft-ROADM with multiple add ports, as shown in Fig. 3(b). Furthermore, the tributary input signal(s) to be added can consist of multiple channels, as the centralised SDN-controller ensures the corresponding wavelength has free channel spaces in the aggregated soft-ROADM input signal.

Optical couplers characteristically support a wide range of operating wavelengths, thus a single OC component type can be utilised for the soft-ROADM add element of all WDM

wavelengths. This facilitates a cost saving advantage due to the associated reduction in component inventory. It should also be noted that the soft-ROADM add operation-induced time delay is negligible which is also highly advantageous when considering the low latency requirements of 5G mobile connections.

2.4 Soft-ROADM drop operation

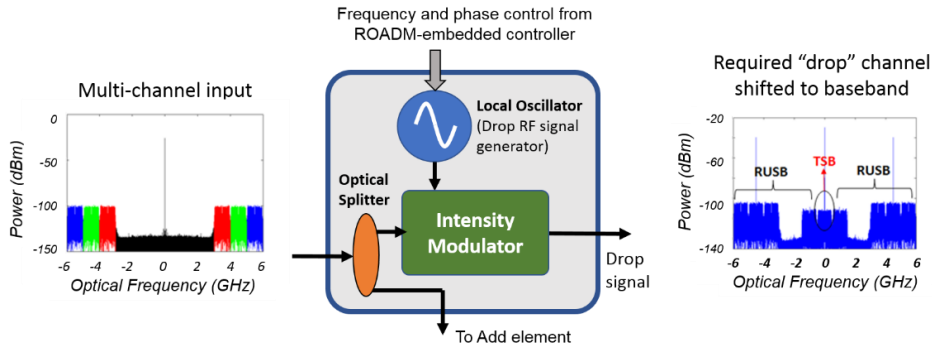

Fig. 4. Soft-ROADM drop element structure with example input and output signal spectra relative to carrier. (TSB: Targeted sub-band. RUSB: Ruined and unrecoverable sub-bands)

In the soft-ROADM drop operation element, as shown in Fig. 4, a 'drop and continue' configuration is adopted as an optical splitter divides the incoming optical signal of a single wavelength into two parts, as mentioned above: one signal passes via an add operation element to form the outgoing signal and the other signal is fed to an optical IM in order to drop the TSB. By driving the IM with a local oscillator (LO)-generated sinusoidal drop RF signal which has both its frequency and phase matched to the TSB, the TSB is down-converted to the baseband spectral region at the IM's output with a spectral reversal occurring. As all Sub-Bs are frequency shifted by $\pm f_{LO}$, where f_{LO} is the LO frequency, the non-targeted Sub-Bs become ruined and unrecoverable Sub-Bs (RUSBs) [13,14] at the output of the drop operation element, these RUSBs are easily eliminated by simple analogue or digital filtering after O-E conversion with similar performances achieved by both filter types [14]. The drop element also has the capability to provide full wavelength level drop functionality simply by driving its IM with a suitable bias voltage and switching off the drop RF signal, the IM then acts as an optical passway.

The remote SDN controller manages the soft-ROADM-embedded controller to set the drop RF signal's frequency and phase [13] according to the channel to be dropped. Fine tracking adjustments of the drop RF signal can be made using pilot signals for detecting optimum performance. The dropped channel's receiver DSP then compensates for the spectral reversal. As the two orthogonal channels have an effective relative phase of 90°, the drop RF signal phase is simply altered by 90° to select the I or Q channel. Some example signal spectra before and after the drop operation are shown in Fig. 4 for an optical wavelength supporting 6 channels. To optimize drop channel performance, the optical signal-to-noise ratio (OSNR) of the dropped signal has to be maximized, this can be conducted by optimising the drop RF signal power [13].

The drop elements 'drop and continue' configuration importantly minimises cost by avoiding optical filtering, but it also allows a multicast function whereby a channel employing different signal modulation formats and multiple access techniques can be dropped at multiple soft-ROADMs and shared by users at different locations in the CAN. Also, due to the low filter complexity enabled, large digital filter space and the fact that the number of cascaded soft-ROADMs in a CAN would not be so high, the non-reuse of channels is not a significant issue for representative application scenarios, as the capacity allocation in the CAN is highly flexible and elastic allowing efficient use of the available filtering space.

Apart from the advantages easily seen from the above description, another advantageous feature of the drop operation is a significant relaxation of required receiver component bandwidths and digital filter complexity, this results in cost and power savings as the receiver detecting the dropped Sub-B only needs to support the channel bandwidth and not the aggregated signal bandwidth. The reduced operating bandwidth can be highly significant, particularly in terms of reducing DAC sample rate requirements and DSP processing power requirements. In a typical CAN the soft-ROADM's drop signals can feed an entire network, thus all ONUs on the network can benefit from the drop operation-induced reduction in operating bandwidth. Furthermore, another key advantage is that the CAN capacity can be incrementally increased by adopting additional channels when required, thus increasing the aggregated bandwidth without the need to upgrade the ONU receivers as the channel bandwidth is unchanged. It should also be noted that, similar to the add operation, the soft-ROADM drop operation-induced latency is also negligible, which is highly advantageous for supporting 5G mobile connections.

3. Real-time transceivers and soft-ROADM experimental system setup

3.1 DSP-based real-time transmitters and receivers

For signal generation and detection, the experiment employs a dual channel, sub-wavelength transmitter and a single channel receiver, each employing a field programmable gate array (FPGA) to implement real-time DSP processing. The DSP architecture is based on the reconfigurable transceiver described in [22], which supports a two channel system and employs Hilbert pair-based digital orthogonal filters for channel multiplexing. In this paper, appropriate modifications are implemented to support a 4 channel system (2 Sub-λ channels each with two Sub-B channels). In the transmitter an up-sampling factor of 4 [17] is adopted and 16 parallel, 64-tap finite impulse response (FIR) filters are used to implement each channel's shaping filter. Also, as filter coefficients are scaled to use the full range of the 8 bit coefficients and as the specific filter impulse response can impact filtered signal amplitude [22], the outputs of the shaping filters pass through on-line adjustable scaling functions to allow the signal amplitudes in each channel to be closely matched. For the matching filter in the receiver, 16 parallel, 64-tap FIR filters are theoretically required, however as a down-sampling factor of 4 is employed, the number of parallel filters physically implemented is reduced to 4. All FIR filters are dynamically software-reconfigurable by on-line reprogramming of the tap coefficients, thus the transmitter filters can be configured as one of four shaping filters, and the receiver filters can also be configured as one of four matching filters or as a LPF for use in the drop operation case.

On each individual channel any signal modulation format would be suitable for the soft-ROADM. Here, for simplicity but without losing any generality, orthogonal frequency division multiplexing (OFDM) is adopted, with pseudo random bit sequences (PRBS) employed as test data. Details of the OFDM parameters are given in Table 1. It should be noted that, in addition to demodulation, the OFDM receiver DSP performs essential functions including symbol alignment and channel equalisation as well as BER analysis for each subcarrier. A slight modification to the OFDM receiver block is also needed for the drop operation demonstration, as it must implement subcarrier conjugation and order reversal to mitigate the drop operation-induced spectral reversal effect.

The employed DACs and ADC are each 8 bit, 2GS/s devices which result in one Sub-λ channel occupying the 0-0.5GHz region, referred to as baseband (BB), and one Sub-λ channel occupying the 0.5-1.0GHz region, referred to as passband (PB). The associated I and Q Sub-Bs are denoted as BB-I, BB-Q, PB-I and PB-Q, respectively. The double-sided amplitude responses of the corresponding 64-tap shaping/matching filters are illustrated in Fig. 5.

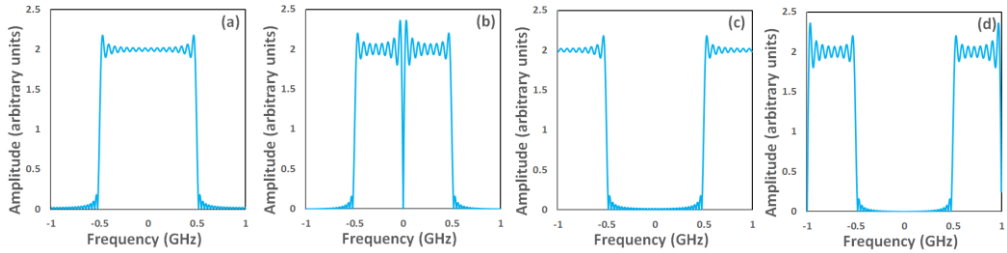

Fig. 5. Shaping and matching filter double-sided amplitude responses (a) BB-I, (b) BB-Q, (c) PB-I, and (d) PB-Q.

3.2 Experimental system setup

Figure 6 shows the soft-ROADM add/drop operation experimental system setup with the adopted experimental system parameters listed in Table 1. Fig. 7 shows examples of Sub-B/Sub-λ and dropped signal electrical spectra measured before and after the soft-ROADM add/drop operations. The adopted transmitter details are shown in Fig. 6(a) for the add operation experiment and Fig. 6(b) for the drop operation experiment. In both Fig. 6(a) and Fig. 6(b), the RF delay lines (DL) after the DACs are required as the entire end-to-end system operation is dependent on correct signal synchronisation. Transmitted signal delays must therefore be adjusted to ensure: i) correct sample timing at the receiver for correct filter operation, and ii) correct relative signal timing between the transmitters to maintain orthogonality when channels to be added are orthogonal with respect to any of the pass-through channels. When channels in different Sub-λ bands are added, their relative transmitter timing is not critical, however the receiver's absolute timing must still be adjusted for each channel independently. The DLs are manually adjusted to achieve optimum sample timing, which gives

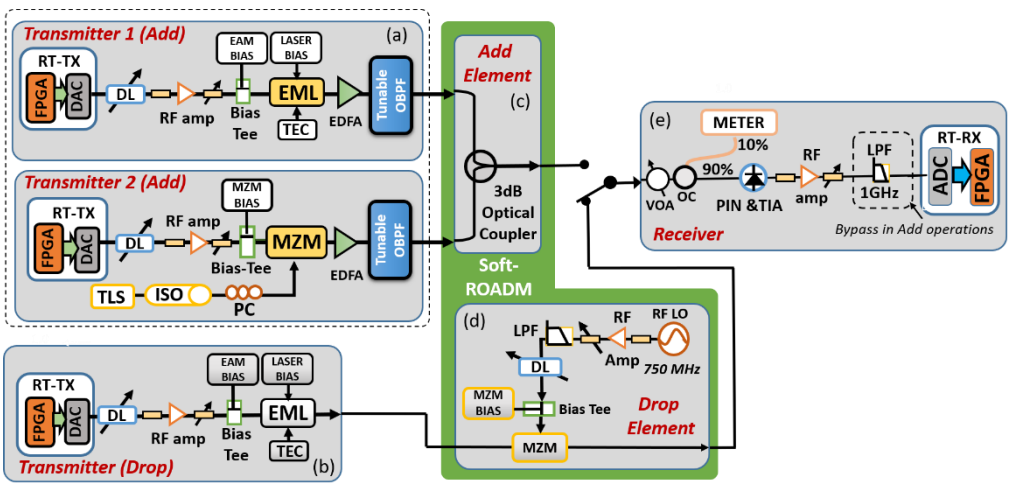

Fig. 6. Soft-ROADM add and drop operations experimental system setup. (a) transmitter system for add operations, (b) transmitter system for drop operation, (c) add element, (d) drop element, and (e) receiver system. DL: Delay line; LPF: low-pass filter; LO: local oscillator; EML: electro-absorption modulated laser; TEC: thermo-electric controller; MZM: Mach-Zehnder modulator; VOA: variable optical attenuator; OBPF: optical bandpass filter; TLS: tunable laser source; PC: polarization controller; PIN+TIA: photodetector with integrated transimpedance amplifier; EDFA: erbium doped fiber amplifier.

rise to minimum BERs for the considered channel. The DL adjustment procedure adopted for all add cases, is to firstly enable a single transmitter and set its DL for minimum BERs on its associated channels, thus attaining correct receiver timing, then the second transmitter is enabled and its DL adjusted for minimum BERs on all channels, thus attaining optimum relative transmitter timing. Moreover, the drop RF signal levels are also adjusted to the

optimum voltage with an RF amplifier and a fixed and variable electrical attenuator in order to drive the optical IM. In addition, the drop RF signals are combined in a bias-Tee with an optimum DC bias voltage for the IMs. In the first transmitter, the IM is an electro-absorption modulated laser (EML) which has an integrated DFB laser as its light source. The DFB laser is optimally biased and its temperature optimised by an external temperature controller. An erbium doped fibre amplifier (EDFA) with a 0.8nm optical band-pass filter (OBPF), amplifies the EML output to control the optical signal power and allow balancing of the powers from both transmitters.

Table 1. Transceiver and system parameters

Parameter	Value
OFDM IFFT/FFT size	32 points
Maximum data carrying OFDM subcarriers per channel	15
add/drop data-carrying subcarriers per sub-band	6/7
Subcarrier modulation format	16-QAM
DAC and ADC sample rate / bit resolution	2GHz /8 bits
FIR filter clock rate	125MHz
OFDM encoder/decoder clock rate	12.5MHz
Data sequence length for error counting	88,500 Symbols
Raw bit rates per add/drop channel	0.3/0.35 Gb/s
Samples per symbol* IFFT/Cyclic prefix/Total	32/8/40 Samples
EML wavelength/modulation bandwidth	~1550nm[&]/10GHz
EML laser bias current/EAM bias voltage	124 mA/-0.75V
EML/MZM driving voltage for Sub-λ add operation	2.3/1.0 Vpp
EML/MZM driving voltage for Sub-B add operation	2.3/0.6 Vpp
MZM DC bias for Sub-λ/Sub-B add operation	1.3/1.47 V
TLS wavelength/MZM modulation bandwidth	~1550nm[&]/20GHz
PIN sensitivity[#]/Bandwidth	-19 dBm /12.4 GHz
Add/drop optical launch power	4.5/3.1 dBm
EML Sub-λ frequency response roll-offs (BB/PB)	8.5/4 dB
MZM Sub-λ frequency response roll-offs (BB/PB)	8/5 dB
Electrical signal amplitude at ADC	300 mVpp
EML/MZM driving voltage for drop operation	2.3/3 Vpp
MZM DC bias for drop operation	1 Vpp

* Before up-sampling and after down-sampling

& wavelength spacing =0.3nm

Corresponding to 10 Gb/s non-return-to-zero data at a BER of 1.0×10^{-9}

The second transmitter is similar to the first except that the IM is implemented with a tuneable laser source (TLS) and a Mach-Zehnder modulator (MZM). After an isolator, a polarization controller prior to the MZM input is adjusted for optimum performance. The MZM is biased at its quadrature point and is fine-tuned during operation to attain the optimum setting. The MZM output power is set via an EDFA with an OBPF. In the add operation experiment, the direct-detection (DD)-induced optical beat interference (OBI) effect can occur when operating at similar nominal wavelengths, a wavelength spacing of 0.3nm is therefore employed between the two light sources, as this is sufficient to eliminate the OBI effect [23].

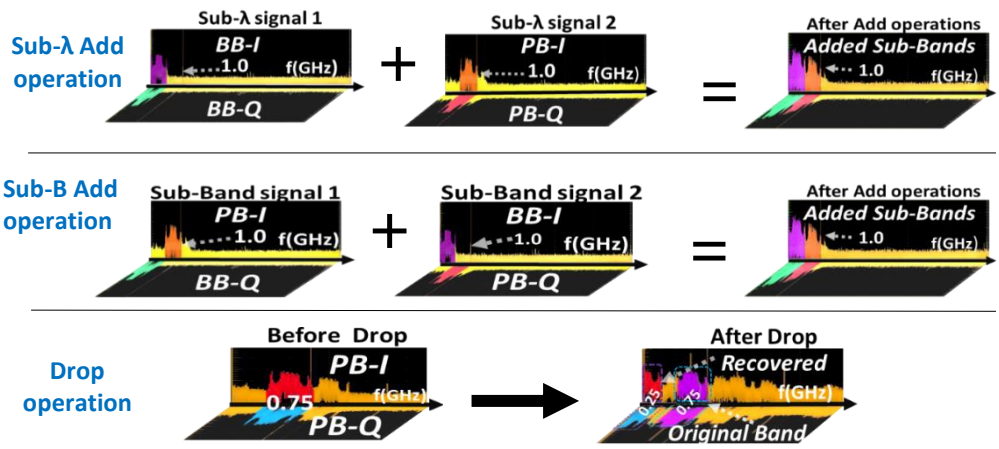

Fig. 7. Representative Sub-λ and Sub-B signal spectra measured before and after the soft-ROADM add/drop operations.

It is also worth noting that the end-to-end optical connections established in the add operation experiments exhibit frequency response roll-off, as detailed in Table 1, which can lead to non-perfect channel orthogonality-induced cross-channel interference (CCI) and subsequent overall system performance degradations [24,25]. This effect is however strictly transmission system-related and not dependent on the soft-ROADM add operation performance.

To configure the soft-ROADM add operation, the add element consisting of a two input 3dB passive optical coupler, as shown in Fig. 6(c), is connected to the outputs of both transmitters in Fig. 6(a), with both transmitters set for an optical output power of 4.5dBm. The output of the add element then feeds the receiver as shown in Fig. 6(e). In the receiver, a variable optical attenuator (VOA) allows the adjustment of received optical power to the required value before direct detection of the optical signal with a PIN+TIA. A coupler is used before the PIN to tap off 10% of the optical power for system monitoring purposes. The electrical signal after the PIN is amplified and variably attenuated to optimise the signal level, before being digitized by the ADC. The samples from the ADC are then processed by DSP implemented in an FPGA as described in Section 3.1. The bit error counts for each OFDM subcarrier are monitored in real-time using the FPGA's embedded logic analyser function. To assess the penalties due to the add operations, before-add (BAD) BER measurements are also made, in conducting this, the optical cables of both transmitters are kept connected to the OC, with both lasers on, then only the considered Sub-λ/Sub-B to be measured is enabled in the DSP. This avoids optical connector-induced power variations and negligible differences are observed in BAD measurements with the unmodulated laser on or disconnected. On the other hand, the after-add (AAD) BER measurements are performed when the Sub-λ/Sub-B channels are simultaneously activated in both transmitters' DSP. To fully examine the soft-ROADM add performance for different add combinations, we define Sub-λ Add as: BB-I+BB-Q optically added to PB-I+PB-Q, and Sub-B Add as: BB-Q+PB-I optically added to BB-I+PB-Q. Furthermore, to examine the add operation robustness to differential optical input power, the gain of the EDFAs in each transmitter in the AAD setup is adjusted to induce a difference in optical signal power at the add element inputs. The impact of differential power on system performance is presented in Section 4.2.

For the drop operation experiment, a single dual-channel transmitter is employed as shown in Fig. 6(b), which generates a PB Sub-λ containing spectrally overlapped and orthogonal PB-I and PB-Q channels. The transmitter is the same as the EML-base transmitter used in the add operation experiment except the EDFA and OBPF are omitted as power balancing is not an issue as there is now only a single transmitter in the experimental setup for the drop operation.

For the before-drop (BDR) case, the transmitter in Fig. 6(b) connects directly to the receiver in Fig. 6(e), thus bypassing the drop element, here data is recovered as in the BAD/ADD case, i.e. using appropriate matching filters. To configure the setup for the soft-ROADM after-drop (ADR) operation, the drop element in Fig. 6(d) is now inserted between the aforementioned transmitter and receiver. The soft-ROADM drop element employs a MZM-based IM with a manually controlled LO for the drop RF signal generation. To drop either Sub-B from the PB Sub-λ, the RF drop signal's frequency is set to the PB Sub-λ CF (0.75GHz). The drop RF signal's amplitude is optimised by an RF amplifier and a variable RF attenuator, and the phase is manually controlled by a variable RF DL to select either the PB-I or PB-Q channel and is finely tuned to give a minimum BER for the dropped channel.

To recover the OFDM signal from the baseband-shifted Sub-B, it is necessary to use an analogue, anti-aliasing, low pass filter with a bandwidth equal to the Nyquist frequency of 1GHz, before the ADC to remove unwanted remaining sub-bands above the Nyquist frequency. The receiver's digital FIR filter is configured as a LPF with a 250MHz bandwidth which corresponds to the bandwidth of the wanted channel located at baseband. The modified OFDM demodulator for signal spectral reversal is also adopted.

To analyse the robustness of the drop operation to drop RF signal variations, manual adjustments are made to its amplitude and phase using a variable electrical attenuator and RF DL respectively, whilst the corresponding variations in drop channel BERs are observed. The impacts of drop RF signal variations on system performance is presented in Section 4.3.

4. Experimental results

The overall BER performance of an established optical connection can be affected by transceiver/system-related effects, including, for example, i) limited filter tap count-induced enhancement of digital filter frequency response ripples; ii) unwanted subcarrier-subcarrier-intermixing (SSI) products [26] generated upon square-law photon detection, and iii) frequency response roll-off-induced CCI between the orthogonal channel pairs. As all of these effects are more predominant for lower frequency subcarriers, to effectively highlight the soft-ROADM operation impairments only, a number of low frequency subcarriers are thus deactivated in each 16-QAM-encoded OFDM signal to ensure that acceptable BER levels for each subcarrier in each Sub-B are always obtainable before and after the soft-ROADM operations. Specifically, the 6 (7) highest frequency subcarriers are employed in each Sub-B for the ROADM add (drop) operations.

4.1 Performance of add and drop operations

Based on the experimental setups and parameters presented in Section 3.2, the BER curves versus received optical power (ROP) of each added signal, measured before and after the add operation for Sub-λ and Sub-B add operations, are shown in Figs. 8(a)-8(b) and Figs. 8(d)-8(e) respectively. For the Sub-λ add case the BB (PB) channels are generated by the EML-based (MZM-based) transmitter, whereas for the Sub-B add case the BB-Q + PB-I (BB-I + PB-Q) channels are generated by the EML-based (MZM-based) transmitter. At the FEC limit of $1x10^{-3}$ the measured Sub-λ and Sub-B add penalties for all channels are summarised in Table 2. The key physical effects impacting the experimentally observed add operation penalties are: i) finite filter length-induced non-perfect digital filter orthogonality with finite out-of-band attenuation, ii) increase in DD-induced SSI products (particularly due to Sub-λ add-induced increases in both signal bandwidth and power) which characteristically have higher power at lower frequencies, iii) residual frequency response roll-off induced CCI between orthogonal channels, and iv) inter-channel sample timing-offset (STO), which causes the higher PB frequencies to suffer higher STO sensitivity. It should also be highlighted that all these aforementioned physical effects are purely dependent on transceiver implementation rather than the soft-ROADM.

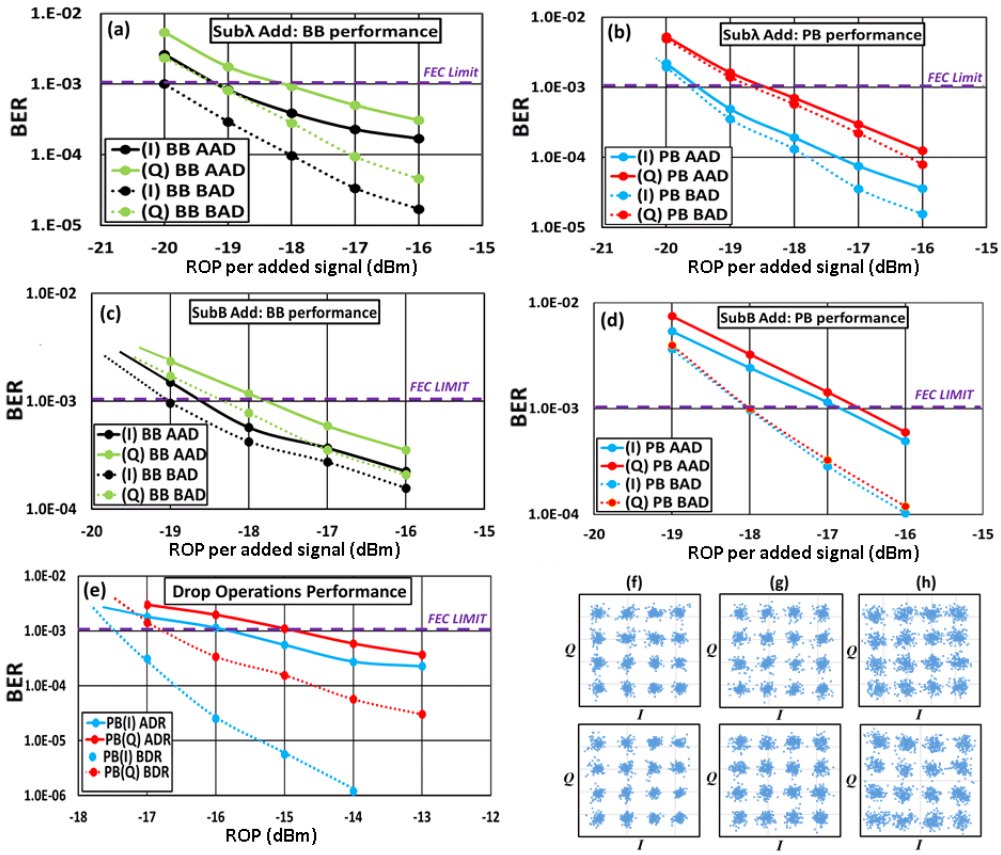

Fig. 8. BER curves for (a),(b) each Sub-B before/after Sub-λ add, (c),(d) each Sub-B before/after Sub-B add, (d) before/after the drop operation; Example subcarrier constellations at -18dBm for the BB-I (upper) and PB-I (lower) after (f) Sub-λ add, (g) after Sub-B add; Example subcarrier constellations at -14dBm after the drop operation for (h) PB-I (upper) and PB-Q (lower).

The SSI products have more impact at lower frequencies which can explain i) the higher penalties observed for BB channels compared to PB channels in the Sub-λ add case, and ii) why BB channels see a higher penalty in Sub-λ add than Sub-B add due to the increased number of intermixing products generated by the doubling of signal bandwidth due to the Sub-λ add operation. The roll off-induced CCI only contributes to the add penalty in the Sub-B add cases as this effect is already present in the Sub-λ add case before the add operation. The exact frequency response profile in each Sub-λ also influences the level of generated CCI. Also, in the Sub-B add case as the orthogonal channels within a Sub-λ originate from different transmitters, their inter-channel STO can be non-zero, thus the resulting CCI contributes to the add penalty. As the PB is more sensitive to STO, this gives rise to the higher penalty observed in the PB for the Sub-B add case.

Figure 8 (c) shows the measured BER curves for the cases of before and after drop operation on PB-I and PB-Q Sub-Bs. As expected from theoretical [14] and experimental [15] results, it can be seen in Fig. 8(c) that the drop operations give rise to similar BER developing trends on both channels. There is also a similar drop penalty of ~2dB for both channels at the adopted FEC limit, which arises mainly due to imperfect MZM-IM transfer function-induced signal distortions [14].

For all of the measured add/drop performances presented in Fig. 8, the Q channel has slightly inferior performance in all cases due to the finite filter length-induced filter frequency response ripples being more prominent for the quadrature filters, as shown in Fig. 5. Similar

behaviours have also been experimentally observed in [15]. Equalized and overlaid example constellations of the received subcarriers for add (BB-I/PBI) and drop (PB-I/PB-Q) cases, at ROPs of -18dBm and -14dBm respectively, are shown in Figs. 8(f)-8(h).

Table 2. Add operation penalties (dB)

	Sub-λ Add		Sub-B Add	
	I	**Q**	**I**	**Q**
BB	0.8	1.0	0.3	0.5
PB	0.1	0.2	1.2	1.4

4.2 Add operation robustness to differential optical input power

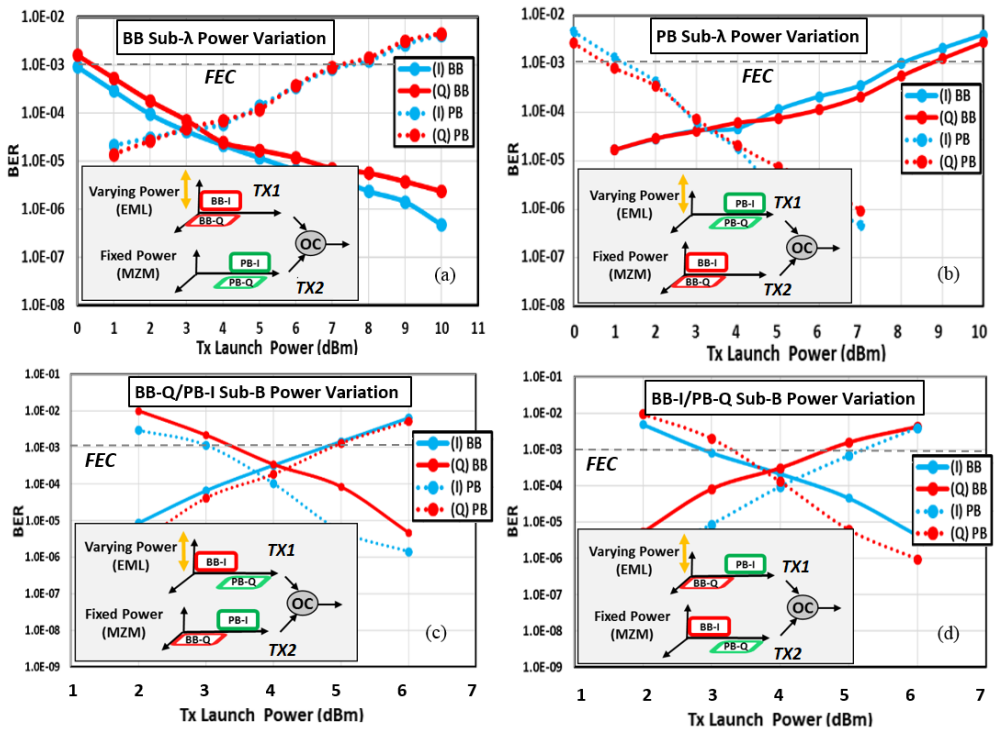

Fig. 9. Differential optical input dynamic range at -10dBm ROP for power variation of: (a) BB Sub-λ (b) PB Sub-λ (c) BB-Q/PB-I Sub-B (d) BB-I/PB-Q Sub-B.

As optical signal power levels can vary within a network, there can be variation between the signal powers present at the soft-ROADM add element ports, it is therefore essential to explore the performance of the soft-ROADM add operation when subject to such power variations in order to evaluate the add operation robustness to differential optical input power. Soft-ROADM Sub-λ/Sub-B add operations can ideally tolerate a large differential optical input dynamic range, which is the maximum variation in the input optical power at one of the add element ports which maintains all channel BERs below a predefined FEC limit.

For all Sub-λ/Sub-B add measurement cases presented in this section, the power of the EML-based transmitter is varied, thus it has a variable optical power (VOP) whereas the MZM-based transmitter has a fixed optical power (FOP) of 4dBm. Furthermore, for all measurements the received optical power is fixed at -10dBm. Figs. 9(a)-9(d) shows the add configurations and the corresponding allowable differential input optical power for Sub-λ/Sub-B add operations. As seen in Fig. 9, two different channel configurations are implemented for each Sub-λ/Sub-B add case so that the effect of power variations on all channels can be explored.

The results in Fig. 9 show that in all cases, as the optical output power of the VOP transmitter increases (decreases) the BER of its associated channels decrease (increases), whereas for the transmitter with FOP the BER of the associated channels increase (decreases). For a FEC limit of $1x10^{-3}$, the observed differential input optical power dynamic range for both Sub-B add cases is ~1.5dB, whereas for the Sub-λ add cases the differential optical input dynamic range is ~6.5dB. As the received optical power is fixed, the dependency of receiver OSNR on transmitted signal powers clearly explains the observed trends of the curves in Fig. 9. The physical mechanism underpinning the lower differential optical input dynamic range for the Sub-B add case is due to the transceiver and transmission link frequency response roll off-induced residual CCI between the orthogonal Sub-Bs [25], thus as the optical power variation induces a corresponding power variation between orthogonal channels in the same Sub-B, this results in increased (decreased) CCI for the lower (higher) power channel, therefore causing a more rapid change in the effective channel OSNRs which leads to the lower differential optical input dynamic range [25]. For the Sub-λ add cases the aforementioned CCI effect is not an issue, so a considerably larger differential optical input dynamic range occurs, this indicates that the observed optical input power dynamic range in the Sub-B add case is not a limitation of the soft-ROADM but a consequence of transceiver/link induced CCI.

It is also worth mentioning the following two aspects: i) The upper limit of the observed differential optical input dynamic range is determined by the minimum OSNR allowed by the fixed-power optical signal, whilst the lower limit of the differential optical input dynamic range is determined by the minimum OSNR allowed by the variable-power signal; ii) As a direct result of the above statement, the ROP at the destination TET has an important impact on the achievable differential optical input dynamic ranges for the add operations. Under practical conditions, our experiments have shown that the differential optical input dynamic range in dB is almost proportional to total ROP in dBm for Sub-λ add operation.

4.3 Drop operation robustness to drop RF signal characteristics

To explore the robustness of the soft-ROADM drop operation to variations in the drop RF signal characteristics, the BER performance of the dropped PB-I and PB-Q channels are measured as the amplitude and phase of the drop RF signal are varied about their optimum values. Using the experimental system setup and parameters for the drop operation as described in Section 3.2 and with a received optical power of -11dBm, Fig. 10(a) shows, with optimum phase setting, how the BER of each dropped channel varies as the drop RF signal amplitude is varied about the optimum value of ~3Vpp. The fundamental principles underpinning the observed results are that as the drop RF signal amplitude is reduced below ~2.5V, the power of the dropped optical signal reduces [12], thus reducing the dropped signal's OSNR at the receiver. Whereas, when increasing drop RF signal amplitudes above ~3.3V, the amplitude dependent non-linearity effect of the IM induces increasing dropped signal distortions. Whilst maintaining both channel BERs below the FEC limit of 1×10^{-3}, the tolerated amplitude variation is 1.4Vpp (1.9Vpp – 3.4Vpp) corresponding to a power variation of ~5dB, thus the soft-ROADM drop operation is exceedingly robust to the drop RF signal amplitude variations. As such it does not require an amplitude control loop or highly precise setting of the drop RF signal amplitude.

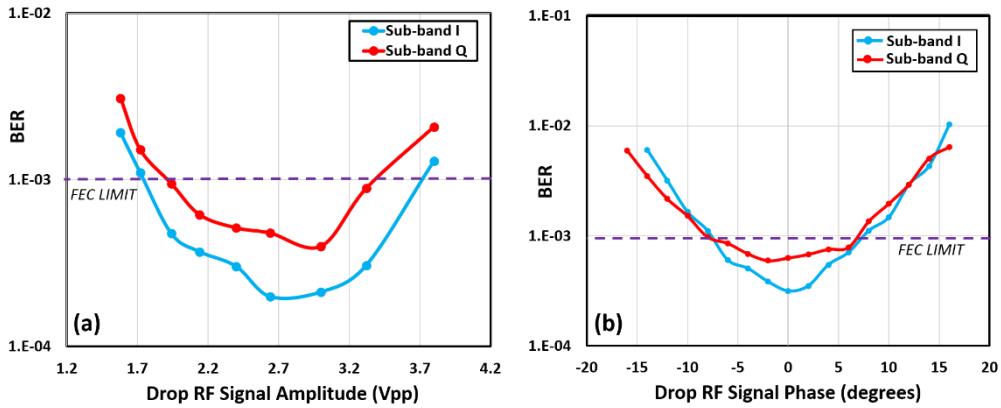

Fig. 10. Variation in soft-ROADM dropped signal BERs (a) as a function of drop RF signal amplitude (b) as a function of drop RF signal phase offset.

With both PB-I and PB-Q channels enabled, Fig. 10(b) shows, with optimum amplitude setting, the BER variation of each dropped channel as the drop RF signal phase is varied about the optimum value for the given channel (shown as 0°). Any deviation from the optimum phase results in phase-offset-induced CCI, as the power from the unwanted orthogonal channel is also down-converted to the baseband spectral region. For the given conditions, the allowed phase offset variation range to maintain BERs below the FEC limit of 1×10^{-3} is ~16°. It should be noted that, similar to the differential optical input dynamic range case presented in Section 4.2, the allowed phase variation range is also dependent on the dropped signal's ROP level, since the BER subject to a zero phase-offset is ROP dependent. However, for a given phase offset there is a fixed ratio of unwanted channel leakage power to wanted channel power, this ratio is ROP-independent, and more predominant at higher ROPs. The relatively shallow slope of the curves in Fig. 10(b) about the optimum phase indicates that the BER has reasonably low sensitivity to phase offset.

Additionally, the level of orthogonality between the two channels in the targeted drop Sub-λ band can also impact the maximum allowed phase variation range, perfect orthogonality being necessary for negligible drop operation-induced CCI, therefore increased filter length-induced improvement in shaping filter characteristics improves channel orthogonality, thus enhancing the allowed phase variation range. As a drop RF signal phase control loop is required to lock to and track the TSB's phase, the observed results show that if a suitable margin is adopted between the zero phase-offset BER and the FEC limit, combined with the very low sensitivity to drop RF signal power, it should be practically feasible to implement the required phase control loop.

5. Conclusions

Making use of DSP-based orthogonal digital filtering, intensity modulation and passive optical coupling, simple, flexible and cost effective soft-ROADMs free from both optical filters and O-E-O conversions have been experimentally demonstrated in a fully real-time 4-channel system. The soft-ROADMs successfully perform DSP-enabled dynamic add and drop operations at sub-wavelength and spectrally overlapped orthogonal sub-band levels. Detailed experimental investigations of the physical-layer add and drop operation performances have been undertaken, the robustness of the add operation to variations in differential optical power and the robustness of the drop operation to variations in the drop RF signal characteristics have also been investigated.

It has been shown that the soft-ROADM introduces maximum optical power penalties as low as 1.4dB for the add operation and 2dB for the drop operation. Furthermore, the results

show the add operation can tolerate a differential optical input dynamic range of 1.5dB (6.5dB) for the Sub-B (Sub-λ) add case. The soft-ROADM drop operation has also been shown to be robust to variations in the drop RF signal characteristics, allowing ~5dBm amplitude variation and 16° of phase variation for the adopted conditions. The very low BER sensitivity to amplitude variations and the observed BER sensitivity to phase offset indicates that it should be practically feasible to implement the required drop RF signal phase control loop.

The fully real-time, proof-of-concept demonstration of the soft-ROADM is a significant step in demonstrating the technical feasibility of the proposed soft-ROADM technology, which can enable cloud access networks to converge fixed and mobile networks supporting key features such as dynamically sliceable networks with ultra-low latency for effective support of 5G mobile networks.

Funding

This work was supported by The Ser Cymru National Research Network in Advanced Engineering and Materials (NRN024); The work of E. Al-Rawachy was supported by the IRAQI Ministry of Higher Education and Scientific Research (MOHESR).